

CONSTITUTIVE-RELATED INSTABILITIES IN PIPE FLOW OF A VISCOELASTIC FLUID

Manuel A. Alves¹

Departamento de Engenharia Química
Centro de Estudos de Fenómenos de Transporte
Faculdade de Engenharia, Universidade do Porto
Rua Dr. Roberto Frias, 4200-465 Porto, Portugal
mmalves@fe.up.pt

Fernando T. Pinho¹

Centro de Estudos de Fenómenos de Transporte
Departamento de Engenharia Mecânica e Gestão Industrial
Faculdade de Engenharia, Universidade do Porto
Rua Dr. Roberto Frias, 4200-465 Porto, Portugal
fpinho@fe.up.pt

Paulo J. Oliveira¹

Departamento de Engenharia Electromecânica
Universidade da Beira Interior
Rua Marquês D'Ávila e Bolama
6200 Covilhã, Portugal
pjpo@ubi.pt

ABSTRACT

The analytical solution for the steady-state flow in a pipe of viscoelastic fluids obeying the complete Phan-Thien—Tanner constitutive equation with a linear stress coefficient is derived. The results include the radial profiles of all relevant stresses, of the axial velocity and of the viscosity. The pipe flow is found to be unstable when the pressure gradient exceeds a critical value determined by a maximum shear rate at the wall. Expressions are also given for the viscometric viscosity and the first and second normal stress difference coefficients, as a function of the shear rate, in steady plane shear flow. For this case, and in line with similar results for the Johnson-Segalman model, the shear stress was found not to be a monotonically increasing function of the shear rate as strong shear-thinning sets in. A new finding is that the critical condition for the maximum shear stress in the simple-shear case is related to the condition for existence of steady-state solution in the pipe flow case. While this may seem evident "a priori" since the pipe flow is a viscometric flow, it is formally demonstrated.

KEYWORDS: Phan-Thien—Tanner fluid, pipe flow.

1. INTRODUCTION

The complete Phan-Thien—Tanner (PTT) constitutive equation was developed from the Yamamoto-Lodge network theory by Phan-Thien and Tanner (1977) using considerations of nonaffine motion of the network junctions relative to the continuum medium. The model is frequently used to model the rheological behavior of polymer melts and is written as

$$Y(\text{tr } \boldsymbol{\tau})\boldsymbol{\tau} + \lambda \frac{\square}{\square} \boldsymbol{\tau} = 2\eta \mathbf{D} \quad (1)$$

where $\boldsymbol{\tau}$ and \mathbf{D} are the extra stress and rate of deformation tensors, λ is a relaxation time and η is the constant viscosity coefficient.

\square

$\boldsymbol{\tau}$ stands for the Gordon-Schowalter convected derivative of the stress tensor $\boldsymbol{\tau}$

$$\frac{\square}{\square} \boldsymbol{\tau} = \frac{D\boldsymbol{\tau}}{Dt} - \boldsymbol{\tau} \cdot \nabla \mathbf{u} - \nabla \mathbf{u}^T \cdot \boldsymbol{\tau} + \xi(\boldsymbol{\tau} \cdot \mathbf{D} + \mathbf{D} \cdot \boldsymbol{\tau}) \quad (2)$$

Parameter ξ accounts for the slip between the molecular network and the continuum medium.

The stress coefficient function has an exponential form (Phan-Thien, 1978)

$$Y(\text{tr } \boldsymbol{\tau}) = \phi(T)f(\text{tr } \boldsymbol{\tau}) = \phi(T)\exp\left(\frac{\varepsilon\lambda}{\eta} \text{tr } \boldsymbol{\tau}\right) \quad (3)$$

which can be accurately linearised for small molecular deformations as occurs in weak flows (according to the flow classification of Tanner, 1985), such as the pipe and pure Couette steady flows dealt with in this paper. The linearised stress coefficient function was proposed in the original paper of Phan-Thien and Tanner (1977) and is given by

$$f(\text{tr } \boldsymbol{\tau}) = 1 + \frac{\varepsilon\lambda}{\eta} \text{tr } \boldsymbol{\tau} \quad (4)$$

Furthermore, as this is an isothermal problem, the thermal function $\phi(T)$ in Eq. (3) is set to 1 following Phan-Thien (1978).

The stress coefficient function introduces a new parameter ε that imposes an upper limit to the elongational viscosity which becomes inversely proportional to ε . When $\varepsilon = 0 \Rightarrow f(\text{tr } \boldsymbol{\tau}) = 1$ and the Johnson-Segalman constitutive equation, used for dilute polymer solutions, is recovered (Larson, 1988). ε can have an influence on the shear properties as well, imparting shear-thinning to the fluid provided its value is not too small (Phan-Thien, 1978 has shown no effect of ε when it is of the order of 10^{-2}).

Viscoelastic duct flows are relevant in polymer processing and simple analytical solutions are preferred to complex calculation routines. Analytical solutions give physical insight into flow

phenomena and can also be used to check results of numerical calculations. A series of analytical solutions for the fully-developed flow of the simplified PTT model ($\xi = 0$) in duct flows have been derived by the authors: channel and pipe flows by Oliveira and Pinho (1999), using both the linear and the exponential forms of the stress coefficient function, and the annular flow solution by Pinho and Oliveira (2000), the latter involving only the linear stress coefficient. Similar solutions for pipe and channel flows with the Giesekus model are presented by Choi et al (1988), Lim and Schowalter (1987) and Schleiniger and Weinacht (1991). For the eight-constant Oldroyd model Deiber and Santa Cruz (1984) derived the velocity profile in pipe flow and similar results for the channel flow of a Johnson-Segalman (JS) fluid with added Newtonian solvent appear in Kolka et al (1988). An implicit analytical solution for the JS fluid in axisymmetric pipe flow was given earlier by Van Schaftingen and Crochet (1985), who expressed the velocity and stress variations in terms of the local shear rates. Pipe and channel flow solutions for simpler viscoelastic models, such as the Upper Convective Maxwell model (UCM), are identical to the corresponding Newtonian solutions presented by Shah and London (1978). Solutions for purely viscous Generalised Newtonian fluids can be found in Bird et al (1987) and Skelland (1967).

This work extends the original paper of Oliveira and Pinho (1999) by presenting the analytical solution for the steady pipe flow of the full PTT model with the linear form of the stress coefficient. This flow is found to be unstable and the conditions for the instability are related to the rheological characteristics of the fluid, that can be determined under controllable flow conditions. Therefore, prior to the presentation of the solution for the pipe flow, the material functions of the PTT model in steady shear flow are presented and discussed.

2. MATERIAL FUNCTIONS

The three shear material functions of relevance are the viscometric viscosity $\mu(\dot{\gamma})$, and the first and second normal stress difference coefficients, $\Psi_1(\dot{\gamma})$ and $\Psi_2(\dot{\gamma})$, respectively, which are obtained in the pure plane Couette flow where the flow is aligned with x (shear rate $\dot{\gamma} = u_{,y}$).

For this flow the constitutive equation (1) is reduced to

$$f(\tau_{ii})\tau_{xx} = \lambda(2 - \xi)\dot{\gamma}\tau_{xy} \quad (5)$$

$$f(\tau_{ii})\tau_{yy} = -\lambda\xi\dot{\gamma}\tau_{xy} \quad (6)$$

$$f(\tau_{ii})\tau_{xy} = \eta\dot{\gamma} + \lambda\left(1 - \frac{\xi}{2}\right)\dot{\gamma}\tau_{yy} - \frac{\lambda\xi}{2}\dot{\gamma}\tau_{xx} \quad (7)$$

with $f(\tau_{ii})$ given by Eq. (4). The trace of the stress tensor is $\tau_{ii} = \tau_{xx} + \tau_{yy}$ and the ratio of Eqs. (5) and (6) gives

$$\tau_{yy} = -\frac{\xi}{2 - \xi}\tau_{xx} \quad (8)$$

Using Eq. (5) for τ_{xy} and Eq. (8) for τ_{yy} , which are introduced into Eq. (7), and after some algebraic manipulations we arrive at

$$\tau_{xx}^3 + a_1\tau_{xx}^2 + a_2\tau_{xx} + a_3 = 0 \quad (9)$$

where

$$\begin{aligned} a_1 &= \frac{\eta(2 - \xi)}{\varepsilon\lambda(1 - \xi)} \\ a_2 &= \frac{\eta^2(2 - \xi)^3\dot{\gamma}^2\xi}{4\varepsilon^2(1 - \xi)^2} + \frac{\eta^2(2 - \xi)^2}{4\varepsilon^2\lambda^2(1 - \xi)^2} \\ a_3 &= -\frac{\eta^3(2 - \xi)^3\dot{\gamma}^2}{4\varepsilon^2\lambda(1 - \xi)^2} \end{aligned} \quad (10 \text{ a,b,c})$$

The real solution of this cubic equation is

$$\tau_{xx}(\dot{\gamma}) = \sqrt[3]{-\frac{\beta}{2} + \sqrt{\frac{\beta^2}{4} + \frac{\alpha^3}{27}}} + \sqrt[3]{-\frac{\beta}{2} - \sqrt{\frac{\beta^2}{4} + \frac{\alpha^3}{27}}} - \frac{a_1}{3} \quad (11)$$

with coefficients

$$\begin{aligned} \alpha &= a_2 - \frac{a_1^2}{3} \\ \beta &= a_3 - \frac{a_1a_2}{3} + \frac{2a_1^3}{27} \end{aligned} \quad (12 \text{ a,b})$$

and is an explicit function of the shear rate $\dot{\gamma}$ and the model parameters, albeit in a complex way.

Further algebraic manipulation gives the desired material functions

$$\mu(\dot{\gamma}) \equiv \frac{\tau_{xy}}{\dot{\gamma}} = \frac{\eta - \lambda\xi\tau_{xx}}{1 + \frac{2\varepsilon\lambda(1 - \xi)}{\eta(2 - \xi)}\tau_{xx}} \quad (13)$$

$$\Psi_1(\dot{\gamma}) \equiv \frac{\tau_{xx} - \tau_{yy}}{\dot{\gamma}^2} = \frac{2\tau_{xx}}{(2 - \xi)\dot{\gamma}^2} \quad (14)$$

$$\Psi_2(\dot{\gamma}) \equiv \frac{\tau_{yy} - \tau_{zz}}{\dot{\gamma}^2} = \frac{-\xi\tau_{xx}}{(2 - \xi)\dot{\gamma}^2} \quad (15)$$

with τ_{xx} given explicitly by Eq. (11).

Xue et al (1998) has given different, but equivalent, expressions for these material functions but have not analysed the shear stress - shear rate behaviour in detail. Such analysis can be separated into two cases which exhibit markedly different behaviour: $\xi = 0$ and $\xi \neq 0$.

For $\xi = 0$ the SPTT model is recovered, as indicated by Eq. (15), for which the second normal stress coefficient is zero. The SPTT model has a shear-thinning behaviour in both the viscometric viscosity and $\Psi_1(\dot{\gamma})$ at intermediate and high shear rates, but constant coefficients at low shear rates. This is shown by the full lines of the shear and normal stress profiles in log-log coordinates of Figures 1 and 2: for the shear stress the low shear rate slope is 1 (constant viscosity), but decreases as $\dot{\gamma}$ increases (shear-thinning); for τ_{xx} the low shear rate slope is equal to 2 (constant Ψ_1) and decreases with shear-thinning.

For $\xi \neq 0$ the constitutive equation exhibits a non-monotonic viscosity behaviour similar to that of a pure Johnson-Segalman fluid (Español et al, 1996; Georgiou and Vlassopoulos, 1998) and, as shown by the dashed lines in Figures 1 and 2, all shear flow characteristics are affected by the value of the slip parameter ξ . Above a critical shear rate ($\dot{\gamma}_c$), defined by the point where the shear stress attains its maximum value, shear-thinning intensity becomes so strong that the slope $d \ln \mu / d \ln \dot{\gamma}$ becomes smaller than -1. This critical shear rate depends on both ξ and ε , and was found here to be given by

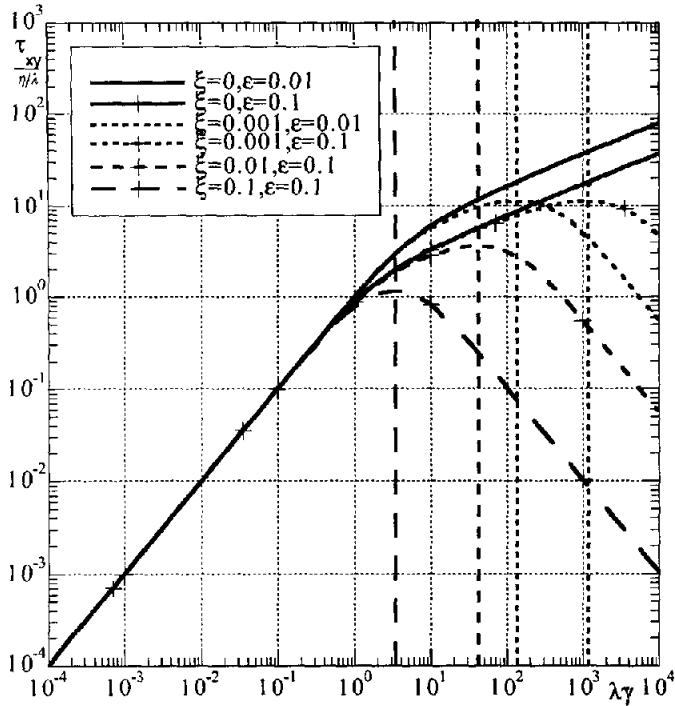


Figure 1- Variation of the shear stress with shear rate in steady Couette flow for a PTT fluid with linear stress coefficient. Vertical lines: $\lambda\dot{\gamma}_c$ of Eq. (19).

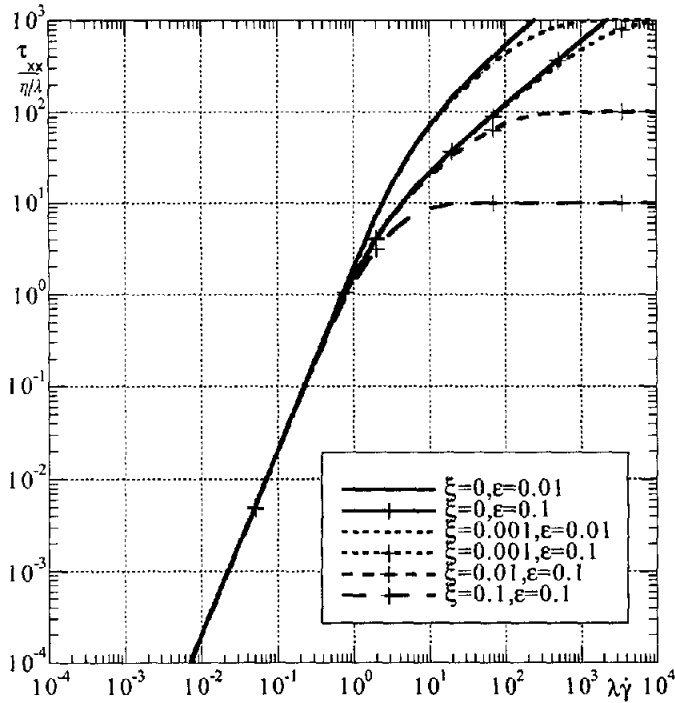


Figure 2- Variation of the streamwise normal stress with shear rate in steady Couette flow for a PTT fluid with linear stress coefficient.

$$\lambda\dot{\gamma}_c = \frac{\epsilon(1-\xi) + \xi(2-\xi)}{[\xi(2-\xi)]^{3/2}} \quad (16)$$

thus tending to occur earlier as either ϵ decreases, or ξ increases. This is also shown in Figure 1 where the vertical lines mark the critical shear rates corresponding to the various cases represented. Expression (16) is an important result which will be derived in a different way from the analysis for the pipe flow presented in the next section.

The corresponding maximum shear stress in plane shear flow is independent of ϵ , as seen in Figure 1, and is given by

$$\left(\frac{\tau_{xy}}{\eta/\lambda} \right)_{\max} = \frac{1}{2\sqrt{\xi(2-\xi)}} \quad (17)$$

The effect of ξ on τ_{xx} is also important and occurs mainly at high shear rates: regardless of the value of ξ , τ_{xx} will tend to a constant value, as shown in Figure 2, and thus $\Psi_1(\dot{\gamma})$ will vary like $\dot{\gamma}^{-2}$. To this variation there is also a contribution of τ_{yy} , but this stress varies in the same way as τ_{xx} following Eq. (8). As Eq. (8) implies τ_{yy} is negative and with ξ taking typically values of 0.2 from experimental data (Huilgol and Phan-Thien, 1997), the absolute value of τ_{yy} does not exceed 15% of τ_{xx} , i.e., $|\Psi_2| \leq 0.1|\Psi_1|$.

3. ANALYTICAL SOLUTION FOR PIPE FLOW

We deal now with the pipe flow of radius R , where the streamwise coordinate and velocity are x and u , and the radial coordinate is r . The coordinate system is centred on the centreline ($r=0$) and the no-slip condition is valid at the wall ($r=R$). In fully-developed flows the velocity and stresses depend only on the radius, the pressure gradient $p_{,x}$ is constant and the continuity equation implies a zero transverse velocity.

The x -momentum equation is independent of the fluid model and can be integrated to give the well known linear variation of shear stress

$$\tau_{xr} = p_{,x} \frac{r}{2} \quad (18)$$

The constitutive equation reduces to the same set of expressions used in the Couette flow, but here it is more convenient to replace $\dot{\gamma}$ by the velocity gradient $u_{,r}$ as velocity is one of the variables of interest. We rewrite Eqs. (5) to (7) as

$$f(\tau_{ii})\tau_{xx} = \lambda(2-\xi)u_{,r}\tau_{xr} \quad (19)$$

$$f(\tau_{ii})\tau_{rr} = -\lambda\xi u_{,r}\tau_{xr} \quad (20)$$

$$f(\tau_{ii})\tau_{xr} = \eta u_{,r} + \lambda \left(1 - \frac{\xi}{2} \right) u_{,r}\tau_{rr} - \frac{\lambda\xi}{2} u_{,r}\tau_{xx} \quad (21)$$

with $f(\tau_{ii})$ given by Eq. (4). Equation (8) is still valid and consequently the function $f(\tau_{ii})$ becomes

$$f(\tau_{ii}) = 1 + \frac{2\epsilon\lambda(1-\xi)}{\eta(2-\xi)} \tau_{xx} \quad (22)$$

Division of Eq. (21) by Eq. (19) results in a second order equation for the streamwise normal stress

$$\lambda\xi\tau_{xx}^2 - \eta\tau_{xx} + \lambda(2-\xi)\tau_{xr}^2 = 0 \quad (23)$$

which has two possible solutions, but only one which is physically realistic: on the symmetry plane ($r=0$) the x -momentum balance (Eq. 18) shows the shear stress to be zero which

implies $\tau_{xx} = 0$ from Eq. (19). This is only possible if the solution to Eq. (23) is the one with the minus sign before the discriminant, i.e.

$$\tau_{xx} = \frac{\eta}{2\lambda\xi} \left[1 - \sqrt{1 - \frac{4\lambda^2\xi(2-\xi)\tau_{xr}^2}{\eta^2}} \right] \quad (24)$$

It is convenient at this stage to introduce a new parameter for compactness

$$a \equiv \frac{-\lambda p_{,x} R}{\eta} \sqrt{\xi(2-\xi)} \quad (25)$$

and, with the shear stress given by Eq. (18) we obtain

$$\tau_{xx} = \frac{\eta}{2\lambda\xi} \left[1 - \sqrt{1 - (ar')^2} \right] \quad (26)$$

where $r' \equiv r/R$ is the dimensionless radial coordinate. In fully-developed flow the pressure gradient is negative and since $\xi \leq 2$ we conclude that the dimensionless parameter a is real and positive. Equation (26) implies the necessity to have $ar' \leq 1$ in order to obtain a real solution for normal stress and, since $r' \leq 1$ such condition implies $a \leq 1$.

Expressions for the normalised stress components are readily obtained after scaling with the wall shear stress for Newtonian (or UCM) fluid. In this process the Deborah number ($De = \lambda U/R$) appears, where U is the bulk velocity. The three nonzero normalised stresses become

$$\begin{aligned} T_{xx} &\equiv \frac{\tau_{xx}}{4\eta U/R} = \frac{1 - \sqrt{1 - (ar')^2}}{8\xi De} \\ T_{rr} &\equiv \frac{\tau_{rr}}{4\eta U/R} = -\frac{1 - \sqrt{1 - (ar')^2}}{8De(2-\xi)} \\ T_{xr} &\equiv \frac{\tau_{xr}}{4\eta U/R} = -\frac{ar'}{8De\sqrt{\xi(2-\xi)}} \end{aligned} \quad (27 \text{ a,b,c})$$

The whole stress field given by Eqs. (18), (24) and (8), for τ_{xr} , τ_{xx} and τ_{rr} respectively, can be substituted into Eq. (19) to give an expression for the radial variation of the shear rate (Eq. 29) below, which may be integrated to yield the velocity profile. In order to improve the readability of the final equations we introduce another parameter χ which combines ε and ξ in a significant way:

$$\chi \equiv \frac{\xi(2-\xi)}{\varepsilon(1-\xi)} \quad (28)$$

The radial profile of shear rate in non-dimensional form is

$$\Gamma(r') \equiv \frac{\dot{\gamma}}{4U/R} = \frac{-1}{4De\sqrt{\xi(2-\xi)}} \left[\left(1 + \frac{2}{\chi} \right) \left(\frac{1}{ar'} - \frac{\sqrt{1 - (ar')^2}}{ar'} \right) - \frac{ar'}{\chi} \right] \quad (29)$$

The radial variation of the viscosity is determined from its definition

$$\mu(\dot{\gamma}) \equiv \frac{\tau_{xr}}{\dot{\gamma}} \Rightarrow \frac{\mu(\dot{\gamma})}{\eta} = \frac{(a)^2 r'}{2 \left[\left(1 + \frac{2}{\chi} \right) \left(\frac{1}{r'} - \frac{\sqrt{1 - (ar')^2}}{r'} \right) - \frac{a^2 r'}{\chi} \right]} \quad (30)$$

and, after integrating Eq. (29) one gets the following dimensional velocity profile

$$u(r) = \frac{\eta}{\lambda^2 \xi (2-\xi) p_{,x}} \left[1 + \frac{2}{\chi} \right] \times \left\{ \ln \frac{1 + \sqrt{1 - (ar')^2}}{1 + \sqrt{1 - a^2}} + \sqrt{1 - a^2} - \sqrt{1 - (ar')^2} \right\} + \frac{p_{,x} R^2}{2\eta\chi} (1 - r'^2) \quad (31)$$

This equation represents a fully analytical solution to the problem of the flow of the complete PTT fluid model through a pipe and it requires knowledge of the applied pressure gradient $p_{,x}$. Often it is the flow rate, or the bulk velocity U , which is known and then it is more convenient to work with the non-dimensional form of Eq. (31) obtained after division by U

$$\begin{aligned} \frac{u(r)}{U} &= -\frac{8}{a^2} \frac{U_N}{U} \left[1 + \frac{2}{\chi} \right] \left\{ \ln \frac{1 + \sqrt{1 - (ar')^2}}{1 + \sqrt{1 - a^2}} + \sqrt{1 - a^2} - \sqrt{1 - (ar')^2} \right\} - \\ &\quad \frac{4}{\chi} \frac{U_N}{U} [1 - r'^2] \end{aligned} \quad (32)$$

In this equation U_N is defined by

$$U_N \equiv -\frac{p_{,x} R^2}{8\eta} \quad (33)$$

and represents the bulk velocity for the flow of a Newtonian fluid subjected to the same pressure gradient. The ratio U_N/U can also be viewed as a dimensionless pressure gradient and, for this case of given U , it is a new unknown of the problem. It can be obtained from integration of the velocity profile over the pipe cross-section, as a result of the standard definition of the bulk velocity

$$U \equiv \frac{1}{R^2} \int_0^R 2ru(r) dr \quad (34)$$

This integration leads to

$$\left(\frac{U_N}{U} \right)^{-1} = \frac{4}{a^2} \left[1 + \frac{2}{\chi} \right] \left\{ 1 - \frac{2}{3} \sqrt{1 - a^2} - \frac{2}{3} \frac{1 - \sqrt{1 - a^2}}{a^2} \right\} - \frac{2}{\chi} \quad (35)$$

However, it is important to realise that equation (35) does not provide an explicit expression for U_N/U since a itself depends on U_N/U as a comparison of Eq. (25) for a and Eq. (33) for U_N shows. In fact it is easy to show that a and U_N/U are related by

$$a = 8 \frac{U_N}{U} De \sqrt{\varepsilon(1-\xi)} \sqrt{\chi} \quad (36)$$

and this expression suggests that we take as two independent parameters a modified Deborah number (defined by $De^* \equiv De \sqrt{\varepsilon(1-\xi)}$) and χ (defined in Eq. 28). These parameters are only unsuitable in the limiting case of $\varepsilon = 0$, when the standard JS fluid is recovered and where one has to revert back to De and ξ .

Hence, Eq. (35) represents a highly non-linear function of two non-dimensional parameters

$$\frac{U_N}{U} = \text{function}(De^*, \chi) \quad (37)$$

which must be solved for U_N/U by numerical means. To this aim we have used a straightforward bisection method and the solution is represented in graphical form to be given and discussed in the next section.

In engineering calculations involving polymer flows in ducts one is often interested in determining pressure drop and pumping capacity, and for this we need an expression for $f Re$, where f is

the Fanning friction factor usually defined as $f \equiv -p_{,x}R/\rho U^2$. The Reynolds number is defined as $Re \equiv \rho U 2R/\eta$ and after some algebra, we arrive at the following expression for fRe

$$fRe = 16 \frac{U_N}{U} \quad (38)$$

This shows that the variation of fRe with De , ε and ξ is proportional to the corresponding variation of the parameter U_N/U and so there is no need to study fRe separately.

4. CONSTITUTIVE INSTABILITY

The real solution for the streamwise normal stress (Eq. 26) was subjected to the condition that $a \leq 1$. As we shall see, the equality $a=1$ leads to a condition corresponding to the onset of a constitutive instability akin to that found for the Johnson-Segalman model and investigated in detail by Español et al (1996) and Georgiou and Vlassopoulos (1998). For this reason we will refer to that condition as representative of "flow instability" even though we cannot offer a physical interpretation for the actual resulting flow; the flow may become unstable and time-dependent, or it may happen that no solution exists.

We start by determining the maximum shear rate in the pipe cross-section, which takes place at the wall ($r=R$). We denote $\dot{\gamma}_{\max} \equiv |\dot{\gamma}_{r=R}|$ and from Eq. (29) we obtain

$$\dot{\gamma}_{\max} = \frac{-\eta}{\lambda^2 \xi(2-\xi)p_{,x}R} \left[\left(1 + \frac{2}{\chi} \right) \left(1 - \sqrt{1-a^2} \right) - \frac{a^2}{\chi} \right] \quad (39)$$

Note the minus sign leading the equation to produce a positive shear rate at the wall. Now, we impose the limiting stability condition $a=1$, together with Eq. (25) to obtain:

$$\dot{\gamma}_{\max,c} = \frac{1}{\lambda \sqrt{\xi(2-\xi)}} \left[1 + \frac{1}{\chi} \right] \quad (40)$$

and finally

$$\lambda \dot{\gamma}_{\max,c} = \frac{1 + \frac{1}{\chi}}{\sqrt{\xi(2-\xi)}} \Leftrightarrow \lambda \dot{\gamma}_{\max,c} = \frac{\varepsilon(1-\xi) + \xi(2-\xi)}{[\xi(2-\xi)]^{3/2}} \quad (41)$$

which is the same equation presented in Section 2 for $\lambda \dot{\gamma}_c$. Hence, the critical shear rate for the maximum of τ_{xr} versus $\dot{\gamma}$ in a simple shear flow ($\dot{\gamma}_c$), is the same as the maximum allowable shear rate in a pipe flow with imposed pressure gradient ($\dot{\gamma}_{\max,c}$). Above this maximum shear rate, the governing equations for the pipe flow do not have a real solution. The constitutive instability due to nonmonotonic shear stress in simple shear is thus connected with conditions for an imaginary solution in the more complex pipe flow.

In his 1958 paper, Oldroyd studied the behaviour of what is now known as the 8-constant Oldroyd model, with view to determine the model parameters that result in predictions of real flow behaviour, such as an apparent viscosity being a decreasing function of the shear rate (his Eq. 54). This is related, but is not equivalent, to studies of flow stability like that of Yerushalmi et al (1970), who have considered the corotational Maxwell model (CRM) with and without a retardation time (i.e. with and without a Newtonian solvent contribution). Yerushalmi et al (1970) have found that flow instability sets in whenever the slope of the flow curve is negative and, for the pure CRM, that happened for shear rates in excess of a

critical value whereas for the corotational Jeffreys model (equivalent to CRM plus a Newtonian solvent), it occurred within a range of shear rates limiting a local maximum and a local minimum in the corresponding flow curve. Thus, the addition of a Newtonian solvent imparts a second critical shear rate at the point where the shear stress exhibits a local minimum.

More recently, these issues have been revived because of the possible link with physical instabilities found in polymer processing flows. It is the case of the spurt phenomena studies of Kolkka et al (1988) and the investigations of shear banding by Español et al (1996) and Georgiou and Vlassopoulos (1998) with the JS model with an added Newtonian viscosity which imparts the second higher critical shear rate associated with a local minimum in shear stress. Although the derivatives used in the CRM and JS constitutive equations are different, the JS fluid suffers from the same shortcomings as the CRM model, hence the effect of adding the retardation time results in the same instability phenomena, leading to the so-called shear banding. The shear banding instabilities exist in this limited range of shear rates where there are multiple solutions to the relationship between the shear stress and shear rate and where the former is a decreasing function of the latter.

In the present work, no retardation time term was added to the PTT model, so there is a single maximum in the shear stress-shear rate curve. If the imposed pressure gradient is such that the wall shear stress exceeds the maximum value, given by Eq. (17), there is no real solution to the steady Poiseuille flow, which may be equivalent in physical terms to the appearance of a different flow, possibly an unsteady flow. Note that the JS model is recovered from the complete PTT model if $\varepsilon=0$, so our findings and the works of Yerushalmi et al (1970), Kolkka et al (1988), Español et al (1996) and Georgiou and Vlassopoulos (1998) suggest that shear banding would also occur for the full PTT fluid with added Newtonian solvent.

Since the constitutive instability is associated with the maximum in the shear stress-shear rate relationship it will always be there provided ξ is nonzero as Figure 1 has already shown. Figure 3 represents the normalised critical shear rate as a function of ξ and ε and shows the stability condition to occur at lower values of the shear rate, as ξ increases and ε decreases. When ξ goes to zero (absence of lower convected derivative in the constitutive equation), $\dot{\gamma}_{\max,c}$ tends to infinity and the flow will be always stable (as found in our previous work, Oliveira and Pinho, 1999). Similarly, the presence of a non-vanishing ε , which brings in some extra degree of shear-thinning relative to the pure Johnson-Segalman fluid, tends to promote stability as the inception of unstable behaviour is shifted to higher values of shear rate. However, parameter ε does not play any role in terms of defining the critical pressure gradient which is given by

$$\frac{(-p_{,x})_c R}{\eta/\lambda} = \frac{1}{\sqrt{\xi(2-\xi)}} \quad (42)$$

rather it acts upon the shape of the velocity profile, making it flatter in the core and steeper at the wall.

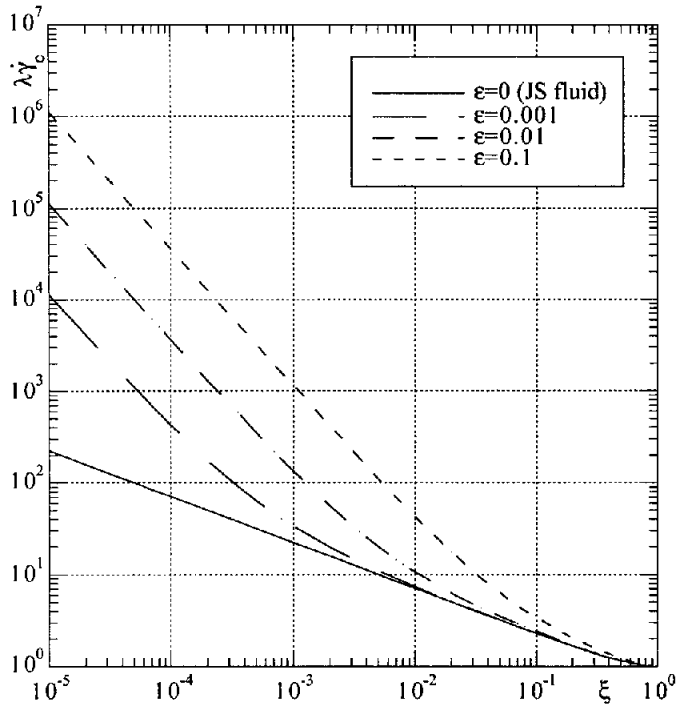


Figure 3- Variation of the critical shear rate with the material parameters ε and ξ .

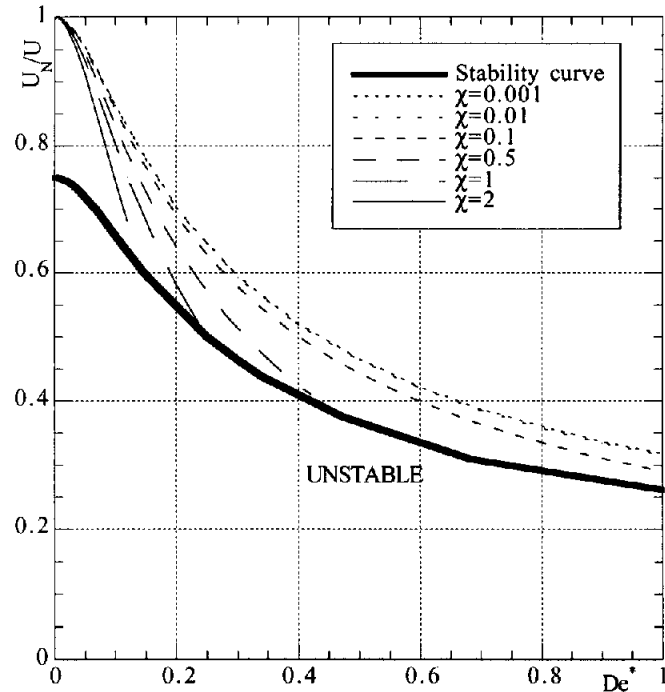


Figure 4- Stability map of the PTT model fluid and ratio of Newtonian and PTT bulk velocities as a function of De^* and χ for pipe flow.

The "stability" condition can also be recast in a different way, involving bulk flow quantities and nondimensional numbers. This results in expressions which are most illuminating for a physical

understanding of the conditions beyond which there are no real solutions to the pipe flow problem. Equation (37) states that the pressure drop for a given flow rate, U_N/U , depends on two parameters, De^* and χ . At the limiting "stability" point the additional condition (42) implies that there remains only a single independent parameter which we may take as De^* or χ , whichever is more convenient. If we equate Eqs. (35) and (36), subject to the stability restraint $a = 1$, we arrive at

$$\left(\frac{U}{U_N}\right)_c \sqrt{\frac{3}{2} \left(\frac{U}{U_N}\right)_c} - 2 = 8De_c^* \quad (43)$$

where De_c^* and $(U_N/U)_c$ denote critical values of De^* and U_N/U . If we plot Eq. (43) in a graph of U_N/U versus De^* we obtain the thick line in Figure 4. This representation can be viewed as a stability map since the region below the thick line (Eq. 43) does not allow for any real solution ("unstable region") and the admissible solutions must be located above that line ("stable region"). In terms of the effect of ξ and ε , an increase in ξ reduces the velocity ratio and narrows the range of permissible solutions whereas ε tends to stabilise the flow.

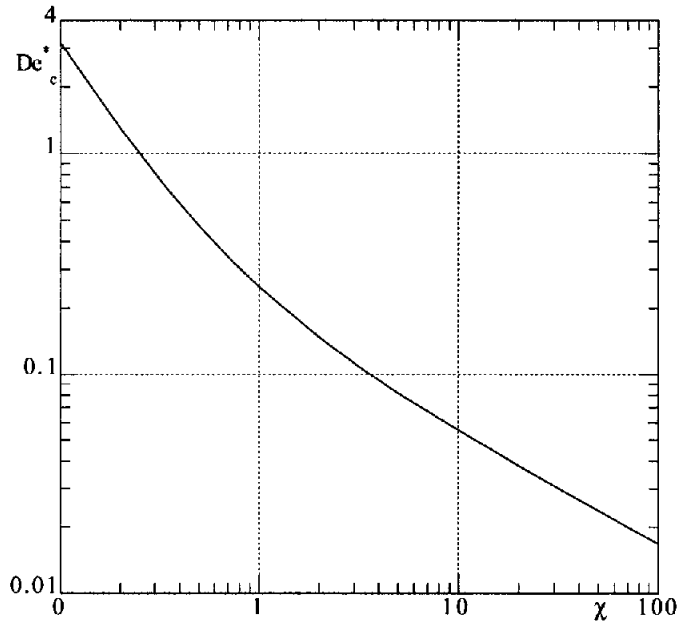


Figure 5- Variation of the modified critical Deborah number with parameter χ for channel and pipe flows.

When De^* tends to zero (negligible elasticity), the critical velocity ratio (or pressure drop) tends to $(U_N/U)_c \rightarrow 3/4$ and when $De^* \rightarrow \infty$, $(U_N/U)_c$ asymptotes to zero. It is also useful to check the limit $\varepsilon \rightarrow 0$ which brings the full PTT model equal to the JS model ($\chi \rightarrow \infty$). To do this we express De_c^* in terms of χ as

$$De_c^* = \frac{1}{6\sqrt{\chi}} \left[1 + \frac{1}{2\chi} \right] \quad (44)$$

and since in this limiting condition it is more adequate to use the standard Deborah number, we introduce the definition of χ (Eq. 31) to get

$$De_c = \frac{1}{6\sqrt{\xi(2-\xi)}} \left[1 + \frac{\varepsilon(1-\xi)}{2\xi(2-\xi)} \right] \quad (45)$$

Application of the limiting condition leading to the JS model ($\varepsilon \rightarrow 0$, $\chi \rightarrow \infty$) we obtain $De_c = 1/6\sqrt{\xi(2-\xi)}$. In the other limit $\xi \rightarrow 0$, $De_c \rightarrow \infty$, i.e., the flow is always stable, as expected (cf Oliveira and Pinho, 1999).

Had we calculated an equivalent expression to Eq. (45) for the channel flow, for which there is also an analytical solution we would arrive at the same result of Kolkka et al for their case without a Newtonian solvent (for further detail see Alves et al, 2001).

The variation of De_c^* with χ of Eq. (44) is given in Figure 5. Each point corresponds to the De^* resulting from the intersection of the permissible U_N/U versus De^* solutions in Figure 4 with the thick stability curve. Figure 5 makes it clear that the range of De for a stable flow becomes wider as χ is reduced, that is as the elongational ε parameter of the PTT model is increased and/or the slip parameter is decreased.

5. DISCUSSION OF PIPE FLOW RESULTS

Within the stable flow region, the thin lines in Figure 4 show the variation of U_N/U with the Deborah number, with χ taken as parameter. The shear-thinning behaviour of the PTT fluid tends to lower the viscosity near the wall compared with the Newtonian fluid and, consequently, for identical pressure gradient the flow rate of the PTT fluid will be higher, i.e., the ratio U_N/U drops with the parameters that enhance shear-thinning, De and χ .

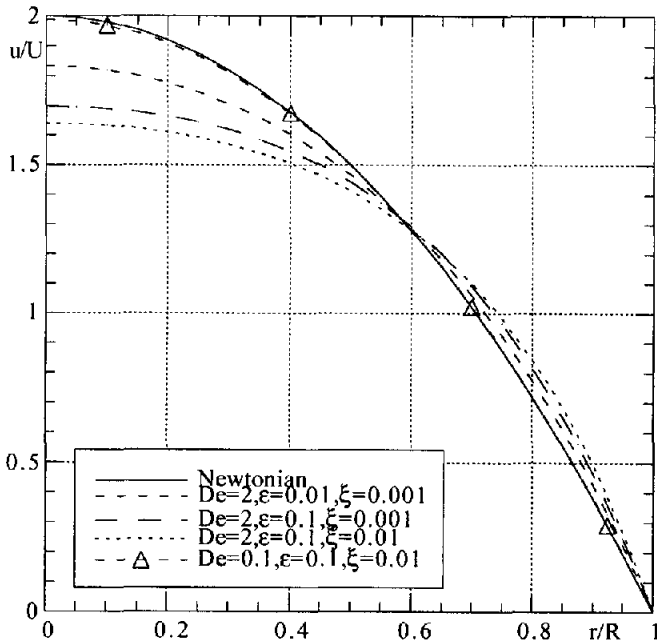


Figure 6- Transverse profiles of axial velocity for pipe flow.

As the ratio U_N/U decreases due to increased shear-thinning the velocity profiles become flatter as shown in the representative plots of Figure 6. The corresponding profiles for the normalised stresses are shown in Figures 7 - 9, for the shear, streamwise

normal and cross-stream normal components, respectively. The figures show separately the effects of Deborah number and of the model parameters ε and ξ .

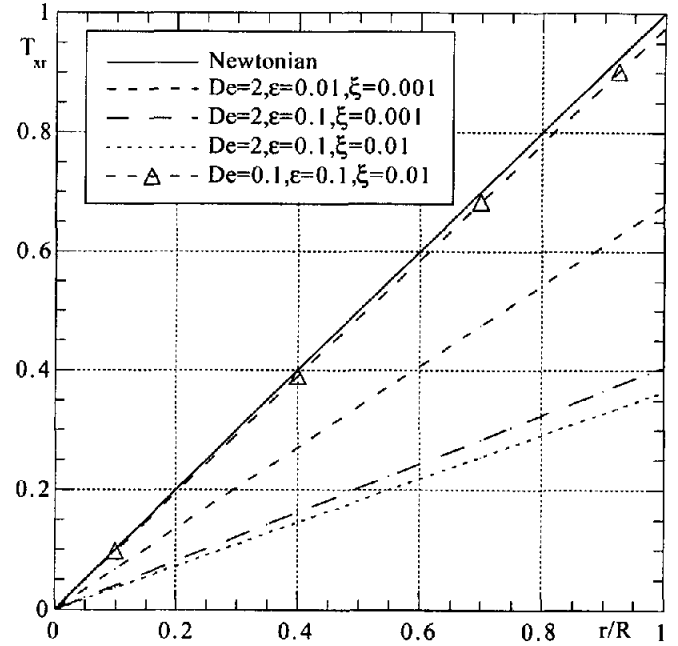


Figure 7- Radial profiles of shear stress for pipe flow.

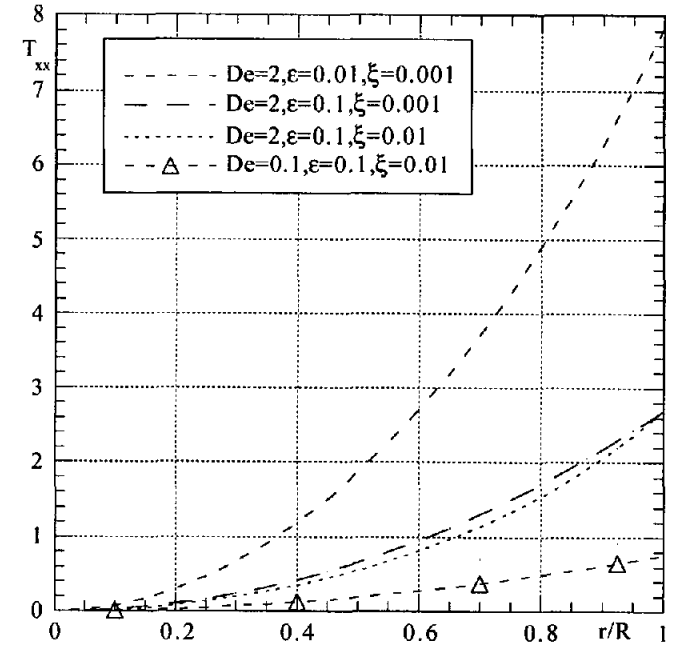


Figure 8- Radial profiles of streamwise normal stress for pipe flow.

The shear stress across the gap must follow a linear variation irrespective of the constitutive equation but its magnitude depends on the model parameters. As seen above, increasing levels of shear-thinning increase the flatness of the velocity profiles and the wall shear rate, thus reducing the wall viscosity and generally

leading to a smaller wall shear stress, or pressure gradient for identical bulk velocity. In this respect, it is noted, from Eqs (27c) and (36), that the dimensionless wall shear stress is equal to $T_w \equiv |T_{xy}(y=1)| = U_N/U$, whose variation was given in Figure 4. The three parameters ε , ξ and λ , the latter via De , all contribute to lower values of $|T_{xy}|$.

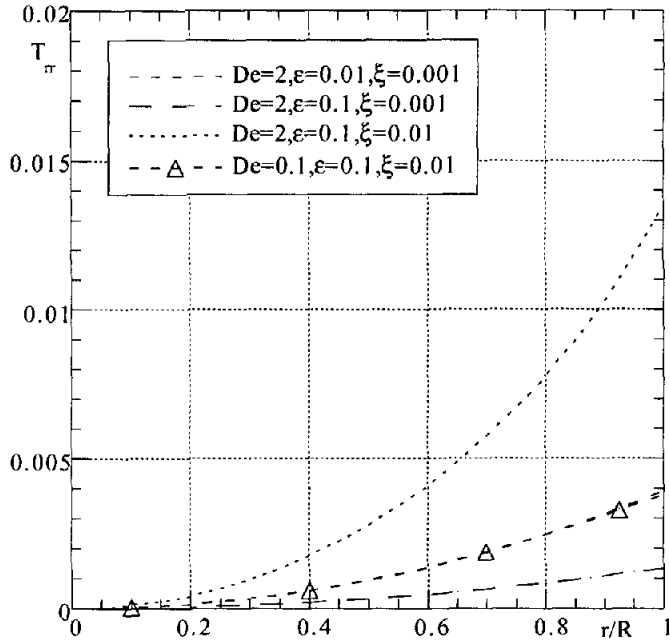


Figure 9- Radial profiles of cross-stream normal stress for pipe flow.

The picture is different for the two normal stresses. With T_{xx} in Figure 8, we see that both ε and ξ contribute to its reduction, with ε imparting a stronger effect than ξ . On the other hand increasing levels of viscoelasticity (higher De) increases this stress component. The transverse normal stress T_{rr} , plotted in Figure 9, is the product of the axial normal stress and a multiplier based on ξ (Eq. 10). It happens that the effect of ξ upon the multiplier is opposite and much stronger to that upon T_{xx} , and consequently T_{rr} increases with ξ whereas T_{xx} decreased.

It is interesting to observe the resulting profiles for a situation on the verge of a critical state. For typical values of the parameters $\xi = 0.2$ and $\varepsilon = 0.1$, which correspond to $\chi = 4.5$, the critical state in pipe flow is at a modified Deborah number of $De_c^* = 0.087297$ ($De_c = 0.30864$) according to Eq. (44). The value $De = 0.308$ ($De_c^* \approx 0.087116$) is just below critical and Figure 10 shows that, although the velocity profile seems absolutely normal, the normal stress T_{xx} is seen to increase sharply near the wall. If the stress components were plotted versus the local shear rate it would be readily apparent that while T_{xx} grows almost linearly with $\dot{\gamma}$, T_{xr} tends to level out showing a maximum near the wall, in agreement with the results for the simple shear flow of Section 2. This differentiated rate of growth of the normal and shear stresses is, however, much clearer if we plot one versus the other,

as in Figure 11. Now we see that the critical situation corresponds to a slope of T_{xx} with T_{xr} tending to infinity; this finding could have been foreseen from Eq. (24), for if we do $(\partial \tau_{xx} / \partial \tau_{xr}) \rightarrow \infty$, we obtain the critical condition under the form of Eq. (42).

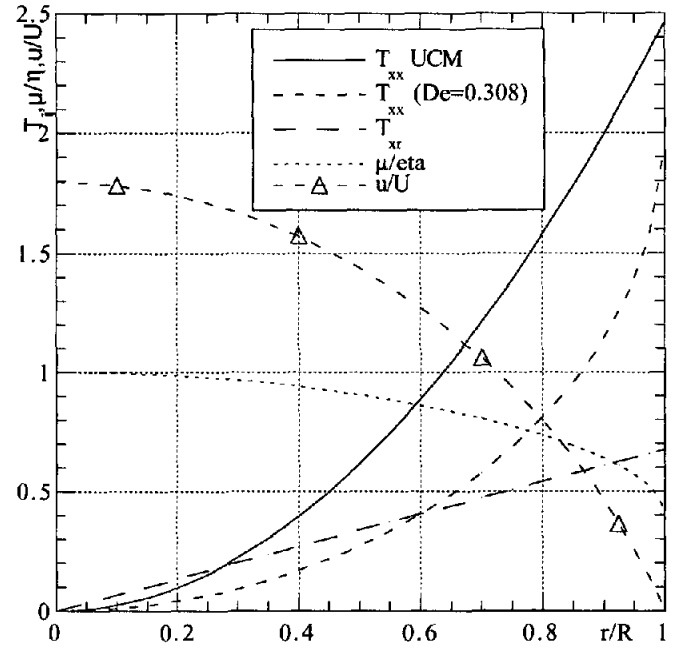


Figure 10- Radial profiles in pipe flow for conditions just below critical at $De = 0.308$ with $\xi = 0.2$ and $\varepsilon = 0.1$.

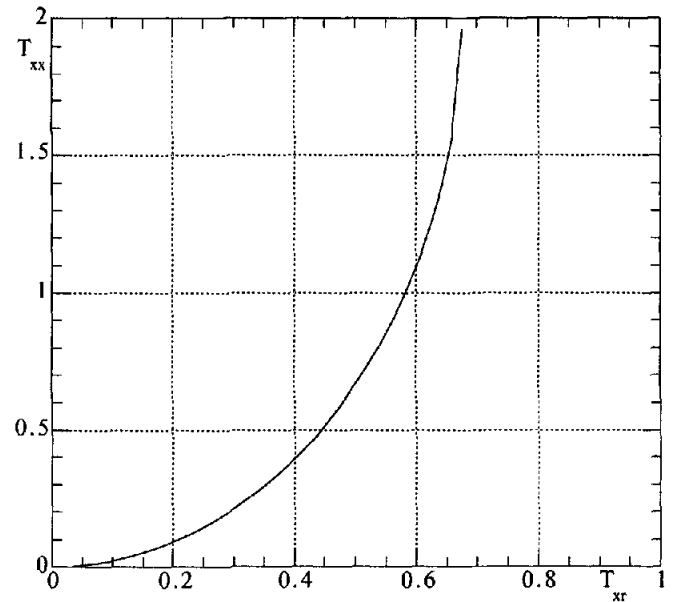


Figure 11- Radial variation of the normal stress with shear stress in the pipe for a situation just below critical ($\xi = 0.2$, $\varepsilon = 0.1$, $De = 0.308$).

6. CONCLUSIONS

An analytical solution is derived for the laminar steady pipe flow of PTT fluids with the linear stress coefficient. The results include the radial profiles of all relevant stresses, of the axial velocity and of the viscosity. Expressions are also given for the viscometric viscosity and the first and second normal stress difference coefficients, as a function of the shear rate, in steady plane shear flow. Similarly to the Johnson-Segalman fluid, the shear stress was found not to be a monotonically increasing function of the shear rate as strong shear-thinning sets in. The critical condition for the maximum in the shear stress-shear rate rheogram is presented.

The pipe flow is found to be unstable when the pressure gradient exceeds a critical value, determined by a maximum shear rate at the wall, and this condition was found to be related to the critical condition in the simple shear flow. The inter-relation between the critical Deborah number in pipe flow, the critical pressure drop (or U_N/U , or wall shear stress) and the modified model parameter χ , was established and discussed. A stability map for the pipe flow was given.

The expressions derived for pipe flow allowed the assessment and discussion of the effects of ε , ξ and De upon the flow hydrodynamics.

REFERENCES

- Alves, M. A., Pinho, F. T. and Oliveira, P. J. 2001. Theoretical study of steady duct flows of the full Phan-Thien—Tanner fluid. Submitted to *J. Non-Newt. Fluid Mech.*
- Bird, R. B., Armstrong, R. C. and Hassager, O. 1987. Dynamics of Polymeric Liquids. Volume 1: Fluid Dynamics, 2nd edition, John Wiley, New York.
- Choi, H. C., Song, J. H. and Yoo, J. Y. 1988. Numerical simulation of the planar contraction flow of a Giesekus fluid. *J. Non-Newt. Fluid Mech.*, vol. 29, pp. 347-379.
- Deiber, J. A. and Santa Cruz, A. S. M. 1984. On non-Newtonian fluid flow through a tube of circular cross section *Lat. Am. J. Chem. Eng. Appl. Chem.*, vol. 14, pp. 19-38.
- Español, P., Yuan, X. F. and Ball, R. C. 1996. Shear banding flow in the Johnson-Segalman fluid. *J. Non-Newt. Fluid Mech.*, vol. 65, pp. 93-109.
- Georgiou, G. C. and Vlassopoulos, D. V. 1998. On the stability of the simple shear flow of a Johnson-Segalman fluid. *J. Non-Newt. Fluid Mech.*, vol. 75, pp. 77-97.
- Huilgol, R. R. and Phan-Thien, N. 1997. Fluid Mechanics of Viscoelasticity, Rheology Series: Volume 6, Elsevier, Amsterdam.
- Kolkka, R. W., Malkus, D. S., Hansen, M. G., Ierley, G. R. and Worthing, R. A. 1988. Spurt phenomena of the Johnson-Segalman fluid and related models. *J. Non-Newt. Fluid Mech.*, vol. 29, pp. 303-335.
- Larson, R. G., 1988. Constitutive Equations for Polymer Melts and Solutions, Butterworths, Boston.
- Lim, F. J. and Schowalter, W. R. 1987 Pseudo-spectral analysis of the stability of pressure-driven flow of a Giesekus fluid between parallel planes. *J. Non-Newt. Fluid Mech.*, vol. 26, pp. 135-142.
- Oldroyd, J. G. 1958. Non-Newtonian effects in steady motion of some idealized elastico-viscous liquids. *Proc. Royal Soc.* vol. A245, pp. 278-297
- Oliveira, P. J. and Pinho, F. T. 1999. Analytical solution for fully-developed channel and pipe flow of Phan-Thien—Tanner fluids. *J. Fluid Mech.*, vol. 387, pp. 271-280
- Pinho, F. T. e Oliveira, P. J. 2000. Axial annular flow of a nonlinear viscoelastic fluid- an analytical solution. *J. Non-Newt. Fluid Mech.*, vol. 93, pp. 325-337.
- Phan-Thien, N. 1978. A nonlinear network viscoelastic model. *J. Rheol.*, vol. 22, pp. 259-283.
- Phan-Thien, N. and Tanner, R. I. 1977. A new constitutive equation derived from network theory. *J. Non-Newt. Fluid Mech.*, vol. 2, pp. 353-365.
- Shah, R. K. and London, A. L. 1978. Laminar Flow Forced Convection in Ducts. Academic Press, New York
- Schleiniger, G. and Weinacht, R. J. 1991. Steady Poiseuille flows for a Giesekus fluid. *J. Non-Newt. Fluid Mech.*, vol. 40, pp. 79-102.
- Skelland, A. H. P. 1967. *Non-Newtonian Flow and Heat Transfer*, John Wiley & Sons, New York.
- Tadmor, Z. and Gogos, C. G. 1979. Principles of Polymer Processing, 1st ed., John Wiley, New York.
- Tanner, R. I. 1985. Engineering Rheology, 1st ed., Clarendon Press, Oxford
- Van Schaftingen J. J. and Crochet, M. J. 1985. Analytical and numerical solution of the Poiseuille flow of a Johnson-Segalman fluid. *J. Non-Newt. Fluid Mech.*, vol. 18, pp. 335-351.
- Xue, S.-C., Phan-Thien, N. and Tanner, R. I. 1998. Three dimensional numerical simulations of viscoelastic flows through planar contractions. *J. Non-Newt. Fluid Mech.*, vol. 74, pp. 195-245.
- Yerushalmi, J., Katz, S. and Shinnar, R. 1970. The stability of steady shear flows of some viscoelastic fluids. *Chem. Eng. Sci.*, vol. 25, pp. 1891-1902.